JOURNAL OF KUFA–PHYSICS
journal.uokufa.edu.iq/index.php/jkp/index | ISSN: 2077–5830

Fano and Dicke Effects in Parallel-Triple Quantum Dots Embedded Between Two Leads

Abbas. A. Hashim, T. A. Salman, and H. A. Jassem

Physics Department, Collage of Science, University of Basrah, Basrah, Iraq

*Corresponding Author E-mail: physicsabbas@gmail.com

ARTICLE INF.

Article history:
Received: 15 SEP., 2023
Revised: 8 JAN., 2024
Accepted: 12 JAN., 2024
Available Online: 24 JUN., 2024

Keywords:

quantum dots
Dicke effect
Fano effect
coupling energy,
Green function

ABSTRACT

This article explores electronic transport in a triple quantum dot system connected in parallel to metallic leads while subjected to an external magnetic flux. The Green-function formalism and the equation of motion approach was employed to derive a comprehensive formula for conductance. The study reveals the presence and modulation of Fano and Dicke effects in the conductance spectra of the Triple quantum dot system (TQD). These effects are controlled by adjusting the interdot coupling energy (t_c), the coupling (Γ) of the three dots to the right and left leads, and manipulating the external magnetic flux.

DOI: https://doi.org/10.31257/2018/JKP/2024/v16.i01.13382

تأثيري ديك وفانو في نقاط كمية ثلاثية متوازية الربط موضوعة بين قطبين

عباس احمد هاشم طالب عبدالنبي سلمان

هيفاء عبدالنبي جاسم

قسم الفيزياء، كلية العلوم، جامعة البصرة، البصرة، العراق

الكلمات المفتاحية:

لنقاط الكمية
تأثير ديك
تأثير فانو،طاقة الاقتران
دالة كرين

الـــخُـــلاصـــة

تبحث هذه المقالة النقل الإلكتروني في نظام النقاط الكمومية الثلاثية المتصلة بالتوازي مع اقطاب معدنية ومعرضة لمجال مغناطيسي خارجي .نحن نستخدم دالة كرين وتقريب معادلة الحركةلايجاة صيغة رياضية تعبر عن التوصيلية في النظام. تكشف دراستنا عن تأثيرات Fano و Dickeفي أنماط التوصيلية لنظام النقاط الكمومية الثلاثية (TQD). يمكن التحكم بالتأثيرن عن طريق ضبط طاقة الاقتران بين النقاط(t_c) ، والاقتران (Γ)بين النقاط الثلاث والقطبينالأيمن والايسر، وكذلك عن طريق معالجة المجال المغناطيسي الخارجي.

1. INTRODUCTION

Interference phenomena in electron transport through multi-quantum dot systems remain asa continual focus of investigation. Such systems, composed of two or more quantum dots coupled to metallic leads, provide an ideal platform for the observable manifestation of interference effects. Among the various quantum interference phenomena observed in quantum dot (QD) systems, the Fano and Dicke effects are particularly intriguing. For instance, in a study by J. Gores andtransport through a quantum dot strongly coupled to electrodes within a two-conduction channel model. Their work demonstrated that the interference of transmitted waves through both channels led to Fano resonance. Furthermore, Piotr Trocha and Józef Barnaś[3] theoretically analyzed spin-dependent transport through two coupled single-level quantum dots affixed to ferromagnetic leads, employing the Green function technique. Their numerical analysis focused on Fano anti-resonance interference and Coulomb interaction effects, revealing a dependence on the sign of the non-diagonal coupling elements. Meanwhile, Chandra Sekhar and others[4] utilized the Dicke effect to enhance the stability and efficiency of CNOT gates and single-qubit gates in quantum computers through concise realizations, In this study, we investigate electronic transport through a triple-quantum dot molecule connected to two leads colleagues [1], the Fano effect was harnessed in a single-electron transistor, leading to the observation of asymmetric Fano resonances in its conductance. These resonances resulted from interference between a resonant and a non-resonant pathway within the system. While the resonant component exhibited typical single-electron transistor behavior, the nature of the non-resonant path remained unclear. Similarly, Bogdan and collaborators[2] delved into electronic.

2. Model

In the context of our study, we have three single-level quantum dots connected to both left and right leads, as depicted in Figure 1. To describe the electronic behavior of these three quantum dots operating in parallel, we extend the single Hamiltonian. This electronic Hamiltonian can be effectively characterized using the Anderson model [5]. Within this model, all coupling interactions between the two dots and between the dots and the two leads were considered. The system's Hamiltonian is thus expressed as follows.

(1)

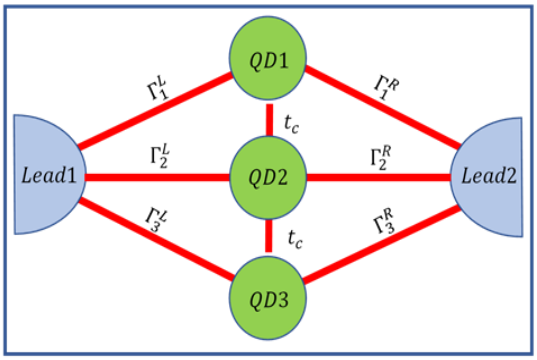

Figure 1: Triple quantum-dot connected in parallel to leads

$$
\begin{aligned}
&H \\
&= H_{Leads} + H_{Dots} \\
&+ H_{Tunneling} \\
&H \\
&= \sum_{k\sigma} \varepsilon_k^L \, a_{k\sigma}^\dagger a_{k\sigma} \\
&+ \sum_{p\sigma} \varepsilon_p^R \, b_{p\sigma}^\dagger b_{p\sigma} \\
&+ \sum_{i\sigma} \varepsilon_i \, c_{i\sigma}^\dagger c_{i\sigma} \\
&+ \sum_{i} U_i \, n_{i\uparrow} n_{i\downarrow} \\
&+ \left[\sum_{k\sigma i} V_{ki}^L \, c_{i\sigma}^\dagger a_{k\sigma} \right. \\
&+ \sum_{k\sigma i} V_{pi}^R \, c_{i\sigma}^\dagger b_{p\sigma} \\
&+ \sum_{\sigma} t_c \left(c_{1\sigma}^\dagger c_{2\sigma} \right. \\
&\left. \left. + c_{2\sigma}^\dagger c_{3\sigma} \right) + H.C. \right]
\end{aligned}
\tag{2}
$$

Where ε_k^L represent thermal kinetic energies of non-interacting free electrons contained in left (right) lead exhibiting band, $a_{k\sigma}^\dagger a_{k\sigma}$ and $b_{p\sigma}^\dagger b_{p\sigma}$ are the creation (annihilation) operators for the electrons in left (right) leads, ε_i is the energy of electron in the discrete energy level on i^{th} dot, $c_{i\sigma}^\dagger (c_{i\sigma})$are electron creation (annihilation) operators on dots, the factor U_i is the on-dot Coulomb interaction for electrons on i^{th} dot (having value relative to other parameter such that dots are in Coulomb blockade regime), $n_{i\sigma} = c_{i\sigma}^\dagger c_{i\sigma}$ represents the occupation number for dots electron. Further, $V_{k(p)i}^{L(R)}$ is the coupling potential of left (right) tunneling barriers with i^{th} dot which are essentially the tunneling matrix. Furthermore, t_c a parameter that represents the inter-dot tunneling coupling between any two adjacent dots.

Neglecting the influence of Coulomb interaction in the dots (i.e $U_i = 0$), then Coulomb term $\sum_i \; U_i \, n_{i\uparrow} n_{i\downarrow} = 0$

Our current study does not take the influence of spin into consideration. However, we may explore this property in the future work, at such point Equation (3) would be modified as follows:

$$
\begin{aligned}
&H \\
&= \sum_{k\sigma} \varepsilon_k^L \, a_{k\sigma}^\dagger a_{k\sigma} \\
&+ \sum_{p\sigma} \varepsilon_p^R \, b_{p\sigma}^\dagger b_{p\sigma} \\
&+ \sum_{i\sigma} \varepsilon_i \, c_{i\sigma}^\dagger c_{i\sigma} \\
&+ \left[\sum_{k\sigma i} V_{ki}^L \, c_{i\sigma}^\dagger a_{k\sigma} \right. \\
&+ \sum_{p\sigma i} V_{pi}^R \, c_{i\sigma}^\dagger b_{p\sigma} \\
&+ \sum_{\sigma} t_c \left(c_{1\sigma}^\dagger c_{2\sigma} \right. \\
&\left. \left. + c_{2\sigma}^\dagger c_{3\sigma} \right) + H.C. \right]
\end{aligned}
\tag{3}
$$

$$
\begin{aligned}
H &= \sum_k \varepsilon_k^L \, a_k^\dagger a_k \\
&+ \sum_p \varepsilon_p^R \, b_p^\dagger b_p \\
&+ \sum_i \varepsilon_i \, c_i^\dagger c_i \\
&+ \left[\sum_{ki} V_{ki}^L \, c_i^\dagger a_k \right. \\
&+ \sum_{pi} V_{pi}^R \, c_i^\dagger b_p \\
&+ t_c \left(c_1^\dagger c_2 + c_2^\dagger c_3 \right) \\
&\left. + H.C. \right]
\end{aligned} \tag{4}
$$

2.1. The Solution of System Kinetic Equation

In order to obtain explicitly the transmission probability $T(\omega)$ and the conductance (G) wewere used the equation of motion approach for the Green's function, then the retarded Green's function is defined by[5];

$$\mathrm{G}_{ij}^r(t) = -i\theta(t)\langle\{c_i(t), c_j^\dagger(t')\}\rangle \tag{5}$$

$\theta(t)$ represent the step function, t' is the initial time which always equal to zero.

Now, we need to obtain the expression for these $(\mathrm{G}^r Fs)$ for parallel configuration of TQDs with the help of the corresponding Hamiltonian given in equation (4)

$$\mathrm{G}_{ij}^r(t) = -i\theta(t)\langle\{c_i(t), c_j^\dagger(0)\}\rangle \tag{6}$$

Where

$$c_i(t) = e^{iHt} \cdot c_i(0) e^{-iHt} \tag{7}$$

By differential equation (4-15), the kinetic equation will be;

$$
\begin{aligned}
&\frac{d}{dt} c_i(t) \\
&= i e^{iHt} [H c_i(0) - c_i(0) H] e^{-iHt} \\
&= i e^{iHt} [H, c_i(0)] e^{-iHt}
\end{aligned} \tag{8}
$$

Substituting equation (4) in equation (8) we obtain:

$$
\begin{aligned}
\frac{d}{dt} c_i(t) = e^{iHt} \Bigg[& -\varepsilon_i c_i \\
& - \sum_{ki} V_{ki}^L \, a_k \\
& - \sum_{pi} V_{pi}^R \, b_p \\
& - t_c c_2 \\
& - t_c c_3 \Bigg] e^{-iHt}
\end{aligned} \tag{9}
$$

Where $\delta_{ij} = \left[c_i, c_j^\dagger\right]$

Deriving equation (5) for retarded Green's function we obtain:

$$
\begin{aligned}
&\frac{d}{dt} \mathrm{G}_{ij}^r(t) \\
&= -i \frac{d}{dt} \theta(t) \langle\{c_i(t), c_j^\dagger(0)\}\rangle \\
&- i\theta(t) \left\langle \left\{ \frac{d}{dt} c_i(t), c_j^\dagger(0) \right\} \right\rangle
\end{aligned} \tag{10}
$$

$$
\begin{aligned}
&i \frac{d}{dt} \mathrm{G}_{ij}^r(t) \\
&= \delta(t)\delta_{ij} \\
&+ \theta(t) \left\langle \left\{ \frac{d}{dt} c_i(t), c_j^\dagger(0) \right\} \right\rangle
\end{aligned} \tag{11}
$$

Where $\delta(t)\delta_{ij} = \frac{d}{dt}\theta(t)\langle\{c_i(t), c_j^\dagger(0)\}\rangle$, putting equation (9) into equation (11), we had the following equation;

$$
\begin{aligned}
i \frac{d}{dt} \mathrm{G}_{ij}^r(t) = \delta(t)\delta_{ij} &+ \varepsilon_i \mathrm{G}_{ij}^r(t) \\
&+ \sum_{ki} V_{ki}^k \, G_{kj}^r(t) \\
&+ t_c G_{2j}^r(t) \\
&+ t_c G_{3j}^r(t)
\end{aligned} \tag{12}
$$

We used Fourier transform for the retarded Green function $G_{ij}^r(t)$ where $i\frac{d}{dt}G_{ij}^r(t) = (\omega + i\eta)G_{ij}^r(\omega)$, then we obtain the following relation;

$$\omega G_{ij}^r(\omega) = \delta(t)\delta_{ij} + \varepsilon_i G_{ij}^r(t) + \sum_{ki} V_{ki}^k G_{kj}^r(t) + t_c G_{2j}^r(t) + t_c G_{3j}^r(t) \quad (13)$$

The term (V_{ki}^k) in equation (13) defined the tunneling matrix elements coupling the i-th dot with right (Lift) leads, for simplicity we replaced it by the magnitude of the matrix element ($|V_{ki}^k| \approx \Gamma_i^k$), the 3rd term will be;

Also t_c will replaced by t_{21} or t_{23} depends on the transition process between the three dots, then we obtained from equation (13) these sequential equations;

$$\omega G_{11}^r = 1 + \varepsilon_1 G_{11}^r + t_{21} G_{21}^r + \Gamma_1^L G_{L1}^r + \Gamma_1^R G_{R1}^r \quad (14)$$

$$\omega G_{12}^r = \varepsilon_1 G_{12}^r + t_{22} G_{22}^r + \Gamma_1^L G_{L2}^r + \Gamma_1^R G_{R2}^r \quad (15)$$

$$\omega G_{13}^r = \varepsilon_1 G_{13}^r + t_{23} G_{23}^r + \Gamma_1^L G_{L3}^r + \Gamma_1^R G_{R3}^r \quad (16)$$

$$\omega G_{21}^r = \varepsilon_2 G_{21}^r + t_{11}^* G_{11}^r + t_{31} G_{31}^r + \Gamma_2^L G_{L1}^r + \Gamma_2^R G_{R1}^r \quad (17)$$

$$\omega G_{22}^r = 1 + \varepsilon_2 G_{22}^r + t_{12}^* G_{13}^r + t_{32} G_{32}^r + \Gamma_2^L G_{L2}^r + \Gamma_2^R G_{R2}^r \quad (18)$$

$$\omega G_{23}^r = \varepsilon_2 G_{23}^r + t_{13}^* G_{13}^r + t_{33} G_{33}^r + \Gamma_2^L G_{L3}^r + \Gamma_2^R G_{R3}^r \quad (19)$$

$$\omega G_{31}^r = \varepsilon_3 G_{31}^r + t_{21}^* G_{21}^r + \Gamma_3^L G_{L1}^r + \Gamma_3^R G_{R1}^r \quad (20)$$

$$\omega G_{32}^r = \varepsilon_3 G_{32}^r + t_{22}^* G_{22}^r + \Gamma_3^L G_{L2}^r + \Gamma_3^R G_{R2}^r \quad (21)$$

$$\omega G_{33}^r = 1 + \varepsilon_3 G_{33}^r + t_{23}^* G_{23}^r + \Gamma_3^L G_{L3}^r + \Gamma_3^R G_{R3}^r \quad (22)$$

The Green functions $G_{Li}^r, G_{Ri}^r (i = 1,2,3)$ that correspond to the coupling of the leads in the above equations are arranged as follows:

$$G_{L1}^r = \Gamma_1^{L*} g_L^r G_{11}^r + \Gamma_2^{L*} g_L^r G_{21}^r + \Gamma_3^{L*} g_L^r G_{31}^r \quad (23)$$

$$G_{L2}^r = \Gamma_1^{L*} g_L^r G_{12}^r + \Gamma_2^{L*} g_L^r G_{22}^r + \Gamma_3^{L*} g_L^r G_{32}^r \quad (24)$$

$$G_{L3}^r = \Gamma_1^{L*} g_L^r G_{13}^r + \Gamma_2^{L*} g_L^r G_{23}^r + \Gamma_3^{L*} g_L^r G_{33}^r \quad (25)$$

$$G_{R1}^r = \Gamma_1^{R*} g_R^r G_{11}^r + \Gamma_2^{R*} g_R^r G_{21}^r + \Gamma_3^{R*} g_R^r G_{31}^r \quad (26)$$

$$G_{R2}^r = \Gamma_1^{R*} g_R^r G_{12}^r + \Gamma_2^{R*} g_R^r G_{22}^r + \Gamma_3^{R*} g_R^r G_{32}^r \quad (27)$$

$$G_{R3}^r = \Gamma_1^{R*} g_R^r G_{13}^r + \Gamma_2^{R*} g_R^r G_{23}^r + \Gamma_3^{R*} g_R^r G_{33}^r \quad (28)$$

Where $g_L^r = \frac{1}{\omega - \varepsilon_L + i\eta}$, $g_R^r = \frac{1}{\omega - \varepsilon_R + i\eta}$

We suppose here that the coupling matrix elements of all the three dots with the leads are equal i.e. $\Gamma_i^R = \Gamma_i^L$ $(i = 1,2,3)$.

Substitute equations (23-28) into equations (14-22) and for simplify, we will restrict our a attention to the particular so the resulting expressions, for G_{ij}^r will be;

$$G_{11}^r(\omega - \varepsilon_1 - \Gamma^2 g) = 1 + (t_c + \Gamma^2 g)G_{21}^r + \Gamma^2 g G_{31}^r \quad (29)$$

$$G_{12}^r(\omega-\varepsilon_1-\Gamma^2 g) = (t_c + \Gamma^2 g)G_{22}^r + \Gamma^2 g G_{32}^r \quad (30)$$

$$G_{13}^r(\omega-\varepsilon_1-\Gamma^2 g) = (t_c + \Gamma^2 g)G_{23}^r + \Gamma^2 g G_{33}^r \quad (31)$$

$$G_{21}^r(\omega-\varepsilon_2-\Gamma^2 g) = (t_c + \Gamma^2 g)G_{11}^r + (t_c + \Gamma^2 g)G_{31}^r \quad (32)$$

$$G_{22}^r(\omega-\varepsilon_2-\Gamma^2 g) = 1 + (t_c + \Gamma^2 g)G_{12}^r + (t_c + \Gamma^2 g)G_{32}^r \quad (33)$$

$$G_{23}^r(\omega-\varepsilon_2-\Gamma^2 g) = (t_c + \Gamma^2 g)G_{13}^r + (t_c + \Gamma^2 g)G_{33}^r \quad (34)$$

$$G_{31}^r(\omega-\varepsilon_3-\Gamma^2 g) = (t_c + \Gamma^2 g)G_{21}^r + \Gamma^2 g G_{11}^r \quad (35)$$

$$G_{32}^r(\omega-\varepsilon_3-\Gamma^2 g) = (t_c + \Gamma^2 g)G_{22}^r + \Gamma^2 g G_{12}^r \quad (36)$$

$$G_{33}^r(\omega-\varepsilon_3-\Gamma^2 g) = 1 + (t_c + \Gamma^2 g)G_{23}^r + \Gamma^2 g G_{13}^r \quad (37)$$

Where the function $g = g_L^r + g_R^r$, and $t^* = t_c$

We started to use the shortened function $y_i(i = 1,5)$ in order to summarize the equation above;

$$(\omega-\varepsilon_1-\Gamma^2 g) = y_1 \quad (38)$$

$$(\omega-\varepsilon_2-\Gamma^2 g) = y_2 \quad (39)$$

$$(\omega-\varepsilon_3-\Gamma^2 g) = y_3 \quad (40)$$

$$(t+\Gamma^2 g) = y_4 \quad (41)$$

$$\Gamma^2 g = y_5 \quad (42)$$

Then equations (29-37) becomes;

$$G_{11}^r y_1 = 1 + y_4 G_{21}^r + y_5 G_{31}^r \quad (43)$$

$$G_{12}^r y_1 = y_4 G_{22}^r + y_5 G_{32}^r \quad (44)$$

$$G_{13}^r y_1 = y_4 G_{23}^r + y_5 G_{33}^r \quad (45)$$

$$G_{21}^r y_2 = y_4 G_{11}^r + y_4 G_{31}^r \quad (46)$$

$$G_{22}^r y_2 = 1 + y_4 G_{12}^r + y_4 G_{32}^r \quad (47)$$

$$G_{23}^r y_2 = y_4 G_{13}^r + y_4 G_{33}^r \quad (48)$$

$$G_{31}^r y_3 = y_4 G_{21}^r + y_5 G_{11}^r \quad (49)$$

$$G_{32}^r y_3 = y_4 G_{22}^r + y_5 G_{12}^r \quad (50)$$

$$G_{33}^r y_3 = 1 + y_4 G_{23}^r + y_5 G_{13}^r \quad (51)$$

Finally, the matrix for the retarded Green's function takes the following form:

$$G_{ij}^r = \frac{1}{A}\begin{bmatrix} y_2y_3 - y_4^2 & y_3y_4 + y_4y_5 & y_4^2 + y_2y_5 \\ y_3y_4 + y_4y_5 & y_1y_3 - y_5^2 & y_1y_4 + y_4y_5 \\ y_4^2 + y_2y_5 & y_1y_4 + y_4y_5 & y_1y_2 - y_4^2 \end{bmatrix} \quad (52)$$

With

$$A = y_1y_2y_3 - y_2y_5^2 - 2y_4^2y_5 - y_1y_4^2 - y_4^2y_3 \quad (53)$$

2.2. Transmission Coefficient Calculation

The transmission rate within a configuration of triple quantum dots delineates the likelihood of an electron traversing through the system, journeying from the left to the right electrode. This crucial parameter substantiates the efficiency of electron conveyance within the parallel arrangement of the triple quantum dots.

In the realm of quantum transmission, the quantification of this transmission rate entails the utilization of the Landauer-Boetecker formalism, as expounded in reference[6]. This method encompasses the computation of the transmission coefficient, an imperative metric denoting the fraction of electrons successfully traversing the quantum dots and attaining the opposite terminus.

The determination of the transmission rate is contingent upon an interplay of intricate factors encompassing electron energy, discrete energy levels, the strength of coupling between quantum dots and between quantum dots and the leads and the magnitude of the applied magnetic field. These multifarious factors intercede to mold the probabilities of tunneling while also orchestrating resonant tunneling phenomena that substantively contribute to the transmission rate. Thus, the transmission rate engenders profound insights into the underlying transport characteristics of the triple quantum dot framework. And we can get the transmission coefficient using the following relation[2, 7-10]:

$$T(\omega) = Tr\{G^A(\omega)\Gamma^R G^R(\omega)\Gamma^L\} \quad (5$$

in which Γ^R, Γ^L represent the various lead-dot tunnel coupling matrix elements and can be represented in the shape of matrices for the parallel TQD systems, as follows:

$$\Gamma^L = \begin{bmatrix} 1 & e^{-i\phi/4} & e^{-i\phi/2} \\ e^{i\phi/4} & 1 & e^{-i\phi/4} \\ e^{i\phi/2} & e^{i\phi/4} & 1 \end{bmatrix} \quad (5$$

$$\Gamma^R = \begin{bmatrix} 1 & e^{i\phi/4} & e^{i\phi/2} \\ e^{-i\phi/4} & 1 & e^{i\phi/4} \\ e^{-i\phi/2} & e^{-i\phi/4} & 1 \end{bmatrix} \quad (5$$

where $\phi = 2\pi\Phi/\Phi_0$ represents the Aharonov-Bohm phase with $\Phi_0 = h/e$ is the flux quantum, and Φ is the magnetic flux.

The values of Γ^R, Γ^L depend on how quantum dots are shaped and arranged. These elements reflect the strength of interaction between quantum dots and nearby leads. In triple quantum dot systems, the arrangement of dots influences these values. Theoretical methods like density functional theory[11] help predict these elements, and experimental techniques like scanning tunneling microscopy[10, 12] provide insights into their behavior. In essence, Γ^R and Γ^L values are shaped by quantum dot geometry, impacting their coupling strengths and potential applications.

3. Results and discussion

In this section, we perform detailed numerical calculations using Matlab simulation to analyze conductance and density of states at zero temperature in symmetrically connected parallel triple quantum dots. We apply the same principles as in chapter three for double quantum dots to understand the factors influencing their behavior. These insights are crucial for developing scalable nanotechnology devices.

In this parallel triple quantum dot setup, three dots are arranged linearly and connected in parallel to two external leads. Electron transport occurs through each dot simultaneously, primarily interacting with the dot they occupy. Transport involves either direct tunneling through a single dot or sequential tunneling through adjacent dots, depending on the interdot coupling strength. Direct tunneling is a single-step process, while sequential tunneling involves hopping between adjacent dots before exiting. Conductance behavior is influenced by interdot coupling (t_c), dot energy levels (ε_i), tunneling coupling

strength with the leads (Γ^i), and external parameters like magnetic fields and temperature. Studying this system helps us understand electron transport mechanisms, quantum interference effects, and how individual dots interact

with external leads. This knowledge is essential for optimizing quantum dot devices used in quantum computing, energy harvesting, and quantum information processing. Additionally, analyzing interdot coupling can help identify conditions for Dicke and Fano effects to emerge.

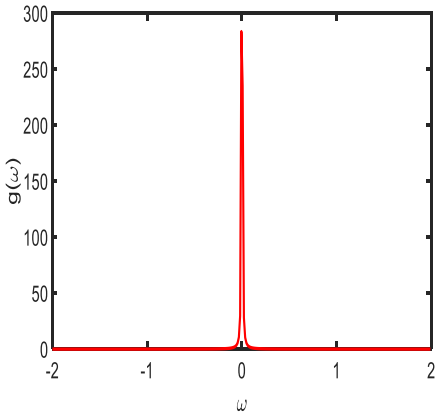

Figure 2: Conductance $\boldsymbol{g(\omega)}$ as a function of energy for $\boldsymbol{\Gamma^L = \Gamma^R = 0.08}$, $\boldsymbol{t_c = 0}$, $\boldsymbol{\phi = 0}$

Additionally, the external parameters, such as the applied magnetic field and temperature, also impact the conductance behavior by affecting the electron tunneling probabilities and energy distribution within the dots. By studying and analyzing the conductance properties of parallel triple quantum dots, researchers can gain insights into the electron transport mechanisms, quantum interference effects, and the interplay between the individual dots and the external leads. Understanding the behavior of this system is essential for

designing and optimizing devices that utilize quantum dots for various applications, such as quantum computing, energy fields and temperature. Studying this system helps us understand electron transport mechanisms, quantum interference effects, and how individual dots interact with external leads. This knowledge is essential for optimizing quantum dot devices used in quantum computing, energy harvesting, and quantum information processing. Additionally, analyzing interdot coupling can help identify conditionsfor Dicke and Fano effects to emerge. Additionally, the external parameters, such as the applied magnetic field and temperature, also impact the conductance behavior by affecting the electron tunneling probabilities and energy distribution within the dots. By studying and analyzing the conductance properties of parallel triple quantum dots, researchers can gain insights into the electron transport mechanisms, quantum interference effects, and the interplay between the individual dots and the external leads. Understanding the behavior of this system is essential for designing and optimizing devices that utilize quantum dots for various applications, such as quantum computing, energy harvesting, and quantum information processing. Also, by carefully examining the interdot coupling between the dots we can gain valuable insights into the conductance behavior at identify the conditions necessary for the emergence of Dicke and Fano effects.

3.1 Conductance

Conductance in a triple quantum dots system signifies the flow of electric current through this unique arrangement of quantum dots. It quantifies how easily electrons move from one electrode to another. The conductance value provides crucial insights into the system's overall electrical behavior, revealing its ability to transport and transmit charge. By studying conductance in triple quantum dots, researchers gain a deeper understanding of electron movement and interactions, which is essential for advancing nanoscale electronics and quantum computing applications[4, 13.[

Our investigation delved into numerically calculating the conductance at zero temperature for triple quantum dots. To ascertain conductance in relation to energy (ω), we utilized the equation below[14-17]

$G(\omega) = (2e\text{^}2)/h\, T(\omega)$ With T(ω) are taken from equation (53).

To illustrate conductivity behavior, we draw Equation (56) against energy in Figure 2, we observe distinct conductivity patterns. When there's no interdot coupling energy t_c and ϕ is zero, a single Fano peak appears at ω = 0, it is known that the Fano effect always disappears in parallel double quantum dots (DODs) system in the absence of magnetic field and when the interdot tunneling t_c is removed. But in our present work and from fig (2) we report a Fano effect in TQDs in parallel configuration even in the absence of magnetic flux.

In fig (3) our conductance calculations are accomplished for t_c=0.4 , $\Gamma\_L = \Gamma\_R = 0.08$ and for different values of external magnetic field ϕ.

From these figs. We clearly notice two set of peaks for each value of ϕ, one is Lorenzian type while another peak is a Fano line shape. Where the appearance of Fano peaks shows the Fano effect occurring due to the quantum interference between discrete levels of the dots and the continuum levels of the leads.

The emergence of a broadening peak and a narrow peak in the conductivity graph within the context of the Fano effect in triple quantum dots can be attributed to the interplay between electron interference and resonance phenomena. Broadening Peak: The broadening peak arises due to the interference between two different electron transport pathways within the triple quantum dot system. In the presence of the Fano effect, one of these pathways becomes more favored, while the other is suppressed. This leads to an enhanced probability of electron transmission through the favored pathway, resulting in a broader, more prominent peak in the conductivity graph. The constructive and destructive interference between these pathways, influenced by the Fano parameter, contributes to the widening of the peak. Narrow Peak: The narrow peak is associated with the resonant tunneling behavior inherent in the Fano effect. Resonant tunneling occurs when the energy levels of the quantum dots align with the energy of the incident electron,

allowing for efficient transmission. In the case of a narrow peak, there is a specific energy alignment that enhances the conductance. This resonance phenomenon accentuates the conductance at that precise energy, leading to the observed narrow peak. However, when discussing pathways and interference in the context of the Fano effect, we are referring to distinct transport routes that electrons can take as they move through the system. In the presence of the Fano effect, the interference between these pathways becomes significant due to the interaction between two main channels :Direct Pathway: This is the most straightforward route for electrons to move through the system. Electrons can directly tunnel from the source lead to one of the quantum dots and subsequently to the drain lead. This path is typically associated with a smooth and broad conductance peak. Resonant Pathway: This pathway involves the resonance of electron energy levels in the quantum dots with the energy of the incident electron. When the energy levels align, electrons can tunnel more efficiently through the system, leading to a sharp and narrow conductance peak. This is the pathway where the Fano effect is most pronounced. At $\phi = 2\pi$, interference vanishes, and the conductance takes a Gaussian distribution. To elucidate ϕ's effect on conductivity, we fix the values of the Γ and coupling energy t_c at certain values while varying ϕ from 0.2π to 0.9π. As ϕ approaches π (Figure 6), the Fano peak emerges. Notably, Fano effects appear at odd number of π and despair in even number of π, resembling Bloch's functions that repeat at specific intervals as shown in figure (4). In Figure 5, we see how coupling energy (t_c) impacts the conductivity graph in a parallel triple quantum dots system, especially in relation to the Fano effect. Higher t_c values lead to a more pronounced and asymmetric conductance peak, which is a key feature of the Fano effect. This asymmetry is shaped by the interplay between direct and resonant tunneling, processes influenced by t_c. Additionally, t_c affects the peak's position, causing shifts to different energy levels, particularly when the Fano effect is active. It also influences the width of the conductance peak, making it narrower and highlighting resonant tunneling behavior. Furthermore, t_c influences interference patterns between electron transport pathways, resulting in a more intricate conductance pattern and contributing to the overall shape of the peak. Increasing t_c amplifies the Fano effect, making it more prominent by affecting the interaction between direct and resonant tunneling pathways. Moving on to Figure 6, we explore the role of the transition rate (Γ) in shaping the conductivity graph. Higher values of Γ lead to a more pronounced and narrower conductance peak because they enhance electron transmission through the resonant pathway. Γ also affects the degree of asymmetry in the peak, making the contrast between symmetric and asymmetric portions more noticeable. Additionally, varying Γ can shift the position of the

conductance peak, altering the graph's resonant behavior.

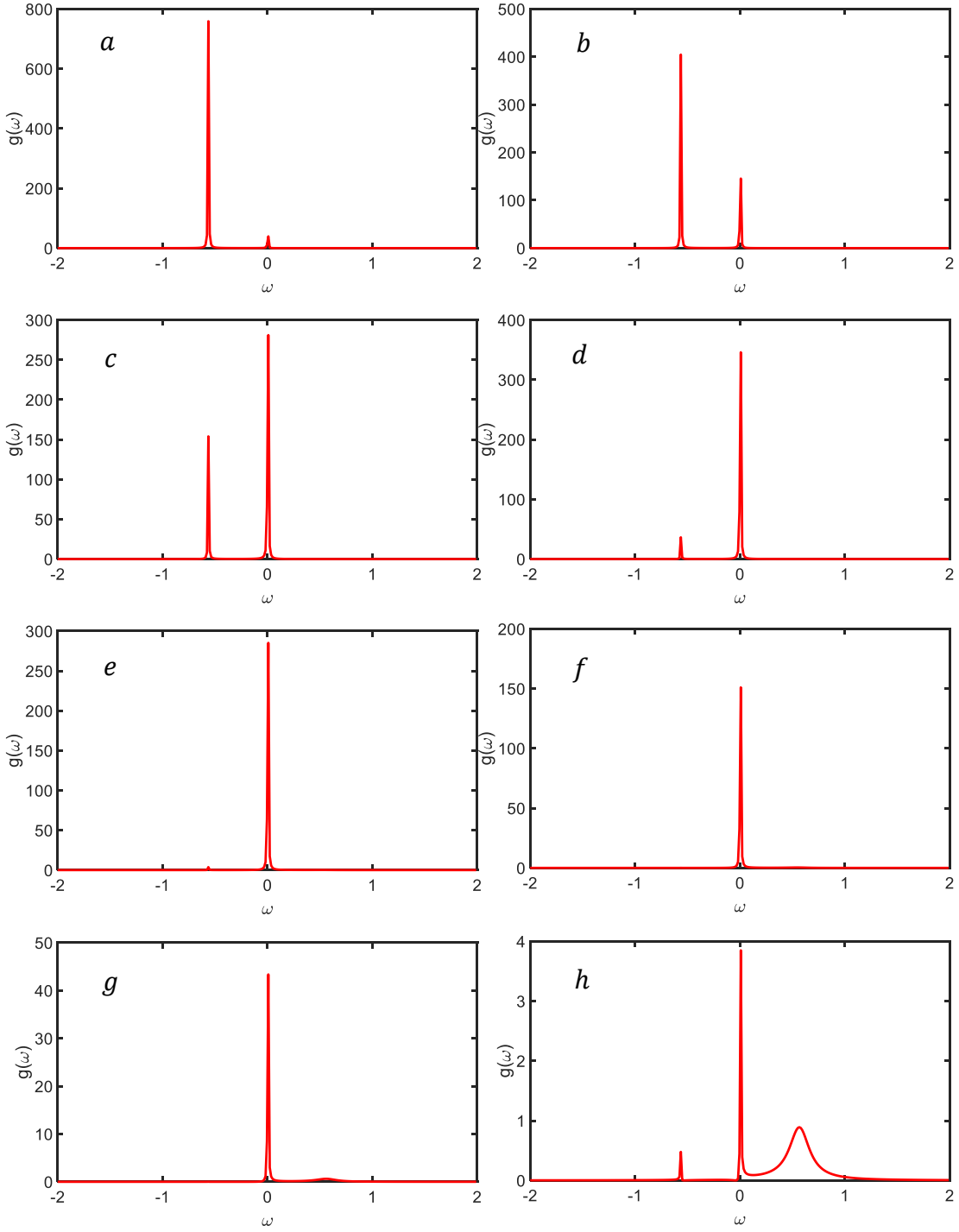

Figure 3: ***Conductance*** $\mathbf{g(\omega)}$ ***as a function of energy and for a different values of*** $\boldsymbol{\phi}$. $\boldsymbol{\Gamma^{L} = \Gamma^{R} = 0.08}$, $\mathbf{t_c = 0.4}$, ***(a)*** $\boldsymbol{\phi = 0.2\pi}$, ***(b)*** $\boldsymbol{\phi = 0.3\pi}$, ***(c)*** $\boldsymbol{\phi = 0.4\pi}$, ***(d)*** $\boldsymbol{\phi = 0.5\pi}$, ***(e)*** $\boldsymbol{\phi = 0.6\pi}$, ***(f)*** $\boldsymbol{\phi = 0.7\pi}$, ***(g)*** $\boldsymbol{\phi = 0.8\pi}$, ***(h)*** $\boldsymbol{\phi = 0.9\pi}$

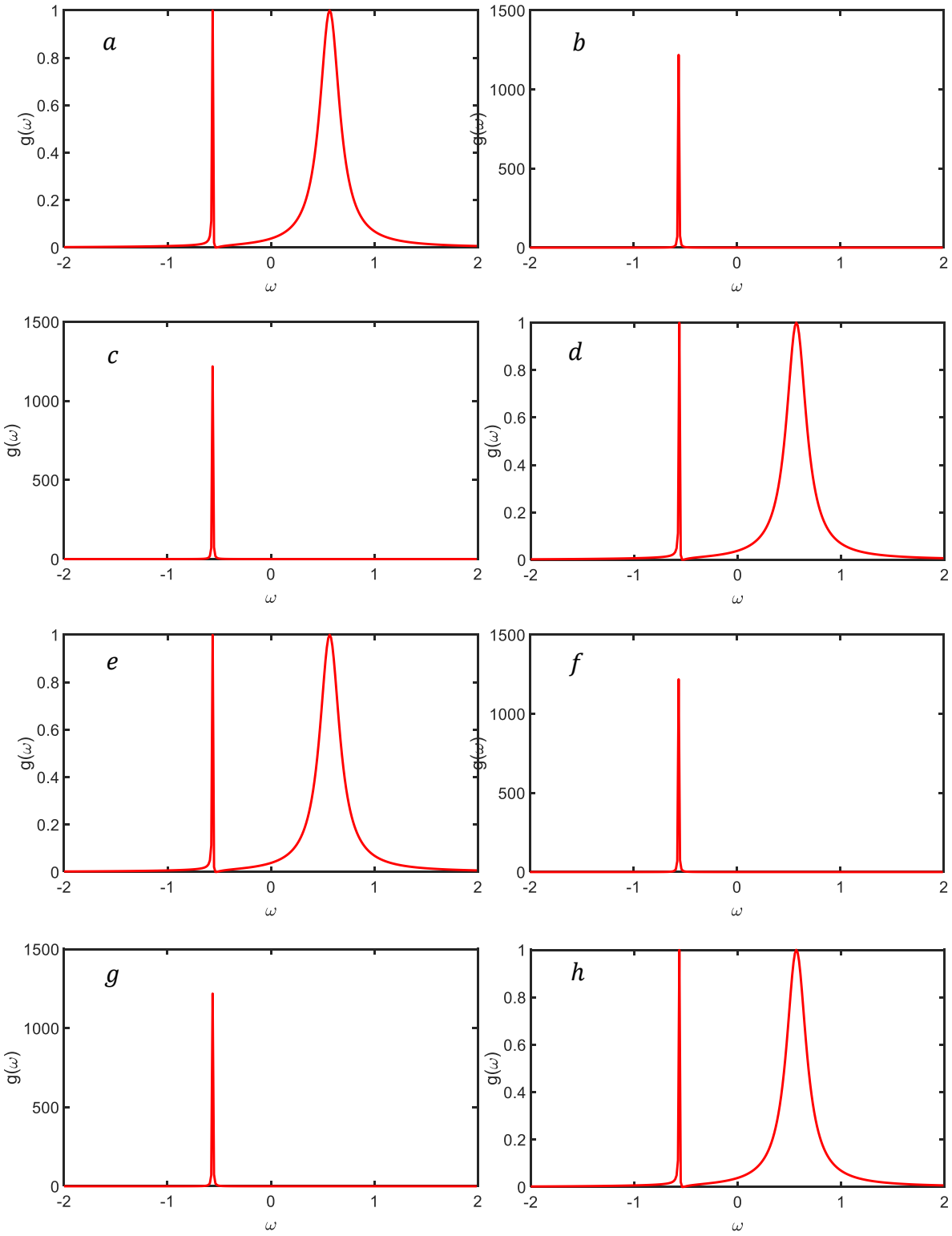

Figure 4: *Conductance* $\mathbf{g(\omega)}$ *as a function of energy and for a different values of* $\boldsymbol{\phi}$. $\boldsymbol{\Gamma^{L} = \Gamma^{R} = 0.08}$, $\boldsymbol{t_c = 0.4}$, *(a)* $\boldsymbol{\phi = 1\pi}$, *(b)* $\boldsymbol{\phi = 2\pi}$, *(c)* $\boldsymbol{\phi = 4\pi}$, *(d)* $\boldsymbol{\phi = 3\pi}$, *(e)* $\boldsymbol{\phi = 5\pi}$, *(f)* $\boldsymbol{\phi = 6\pi}$, *(g)* $\boldsymbol{\phi = 8\pi}$, *(h)* $\boldsymbol{\phi = 7\pi}$

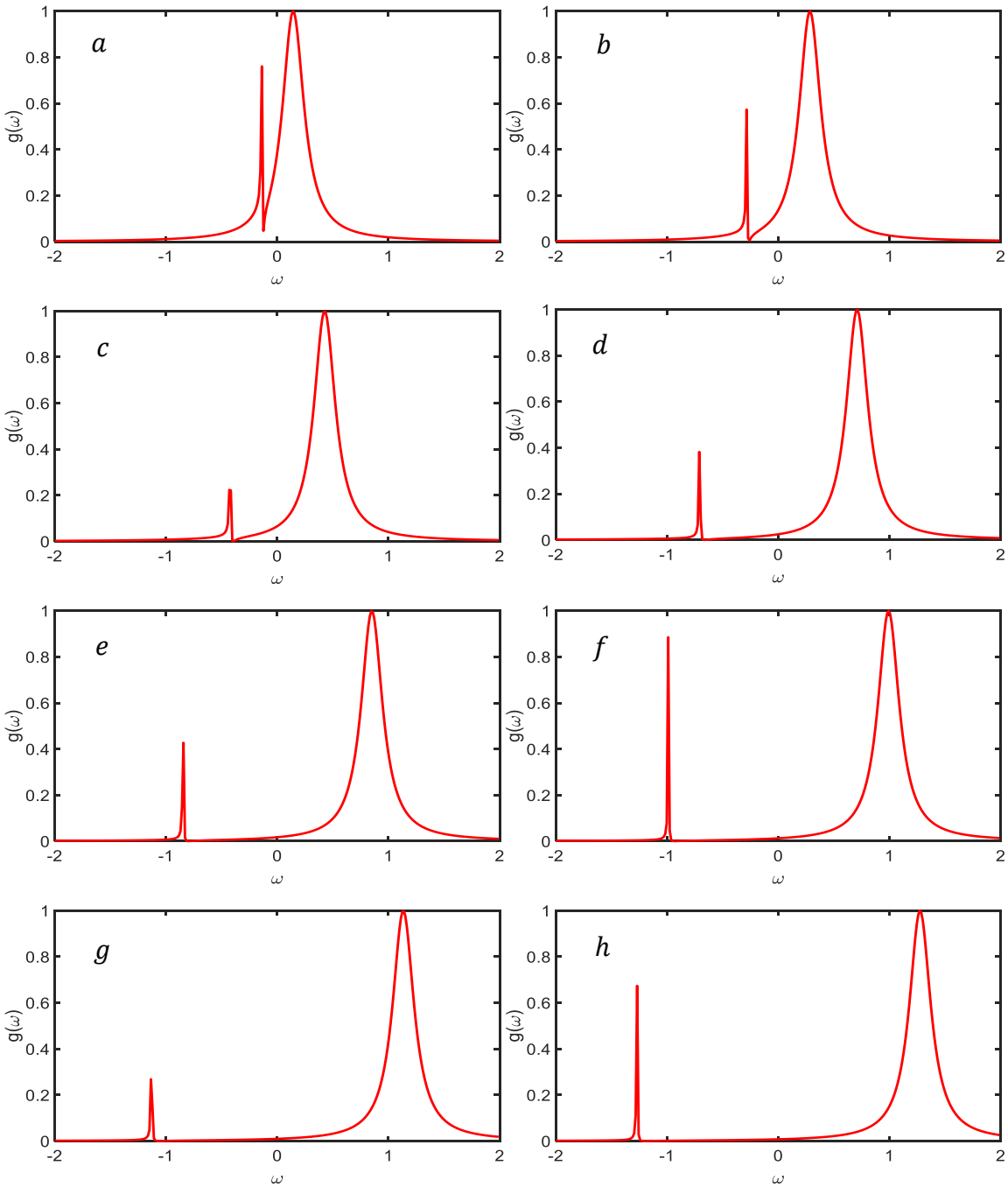

Figure 5: ***Conductance*** $\mathbf{g(\omega)}$ ***as a function of energy and for a different values of*** $\mathbf{t_c}$. $\mathbf{\Gamma^L = \Gamma^R = 0.08}$, $\boldsymbol{\phi = \pi}$, ***(a)*** $\mathbf{t_c = 0.1}$, ***(b)*** $\mathbf{t_c = 0.2}$, ***(c)*** $\mathbf{t_c = 0.3}$, ***(d)*** $\mathbf{t_c = 0.5}$, ***(e)*** $\mathbf{t_c = 0.6}$, ***(f)*** $\mathbf{t_c = 0.7}$, ***(g)*** $\mathbf{t_c = 0.8}$, ***(h)*** $\mathbf{t_c = 0.9}$.

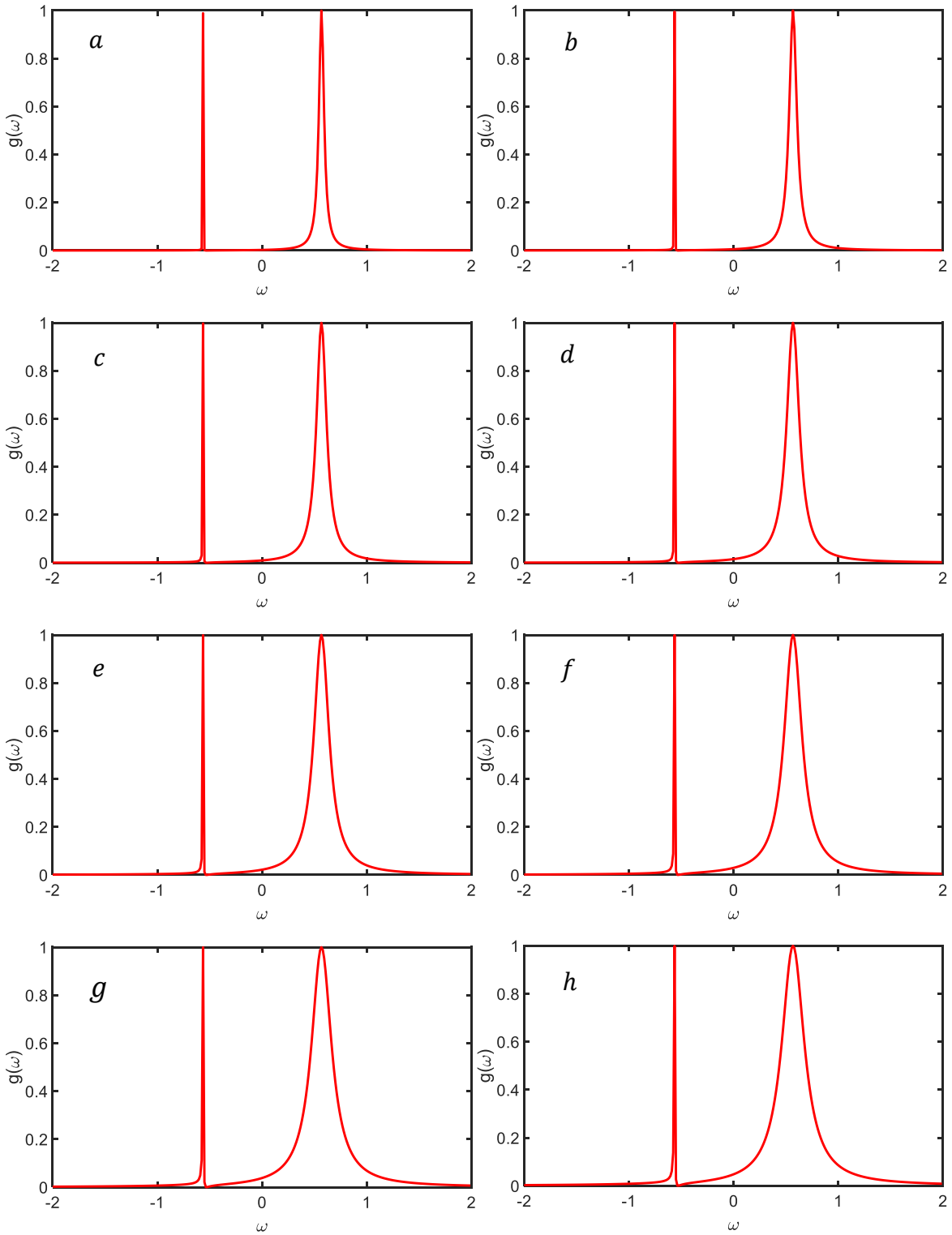

Figure 6: *Conductance* $\mathbf{g(\omega)}$ *as a function of energy for a different values of* $\boldsymbol{\Gamma^{L}}$. $\mathbf{t_c = 0.1}$, $\boldsymbol{\phi = \pi}$, *(a)* $\boldsymbol{\Gamma^{L} = \Gamma^{R} = 0.02}$, *(b)* $\boldsymbol{\Gamma^{L} = \Gamma^{R} = 0.03}$, *(c)* $\boldsymbol{\Gamma^{L} = \Gamma^{R} = 0.04}$, *(d)* $\boldsymbol{\Gamma^{L} = \Gamma^{R} = 0.05}$, *(e)* $\boldsymbol{\Gamma^{L} = \Gamma^{R} = 0.06}$, *(f)* $\boldsymbol{\Gamma^{L} = \Gamma^{R} = 0.07}$, *(g)* $\boldsymbol{\Gamma^{L} = \Gamma^{R} = 0.08}$, *(h)* $\boldsymbol{\Gamma^{L} = \Gamma^{R} = 0.09}$.

4. Conclusion

Understanding how Fano and Dicke's effects are created is crucial for manipulating and harnessing their properties effectively. By exploring their formation mechanisms, researchers can devise strategies to control and optimize these effects for various applications. Furthermore, the significance of the Fano and Dicke effects in modern applications will be underscored. These effects have proven to be instrumental in various fields such as quantum computing, quantum communication, and nanoelectronics. By comprehending their implications, researchers and engineers can leverage these effects to develop advanced technologies and enhance existing systems.

Acknowledgment

References:

[1] J. Göres *et al.*, "Fano resonances in electronic transport through a single-electron transistor," *Physical Review B*, vol. 62, no. 3, p. 2188, 2000.

[2] B. R. Bułka and P. Stefański, "Fano and Kondo resonance in electronic current through nanodevices," *Physical review letters*, vol. 86, no. 22, p. 5128, 2001.

[3] P. Trocha and J. Barnaś, "Quantum interference and Coulomb correlation effects in spin-polarized transport through two coupled quantum dots," *Physical Review B*, vol. 76, no. 16, p. 165432, 2007.

[4] C. S. Mukherjee, S. Maitra, V. Gaurav, and D. Roy, "Preparing dicke states on a quantum computer," *IEEE Transactions on Quantum Engineering*, vol. 1, pp. 1-17, 2020.

[5] J. Anderson, "Bloch functions: The basic theory," *Operators and function theory*, pp. 1-17, 1985.

[6] H. M. Pastawski, "Classical and quantum transport from generalized Landauer-Büttiker equations. II. Time-dependent resonant tunneling," *Physical Review B*, vol. 46, no. 7, p. 4053, 1992.

[7] Y. Liu, X. Hong, J. Feng, and X. Yang, "Fano-Rashba effect in thermoelectricity of a double quantum dot molecular junction," *Nanoscale research letters*, vol. 6, no. 1, pp. 1-10, 2011.

[8] V. Apel, P. Orellana, and M. Pacheco, "Fano and Dicke effects and spin polarization in a double Rashba-ring system side coupled to a quantum wire," *arXiv preprint arXiv:0803.4014*, 2008.

[9] S. Chand, G. Rajput, K. Sharma, and P. Ahluwalia, "Inter-dot coupling effects on transport through correlated parallel coupled quantum dots," *Pramana*, vol. 72, no. 5, pp. 887-902, 2009.

[10] W.-K. Zou, Q. Wang, and H.-K. Zhao, "Dynamic heat and charge transports through double-quantum-dot-interferometer modulated by Majorana bound states and time-oscillating Aharonov-Bohm flux," *Journal of Physics: Condensed Matter*, vol. 35, no. 16, p. 165303, 2023.

[11] P. Hyldgaard, "Density-functional theory of nonequilibrium tunneling," *Physical Review B*, vol. 78, no. 16, p. 165109, 2008.

[12] J. Tersoff and D. R. Hamann, "Theory of the scanning tunneling microscope," *Physical Review B*, vol. 31, no. 2, p. 805, 1985.

[13] F. F. Flöther, "The state of quantum computing applications in health and medicine," *arXiv preprint arXiv:2301.09106*, 2023.

[14] Y. Li, "Fano resonance and flux-dependent transport through a triple-arm Aharonov–Bohm interferometer under an applied electric field," *Journal of Physics: Condensed Matter*, vol. 19, no. 49, p. 496219, 2007.

[15] P. F. Bagwell and T. P. Orlando, "Landauer's conductance formula and its generalization to finite voltages," *Physical Review B*, vol. 40, no. 3, p. 1456, 1989.

[16] Y. Takane and H. Ebisawa, "Conductance formula for mesoscopic systems with a superconducting segment," *Journal of the Physical Society of Japan*, vol. 61, no. 5, pp. 1685-1690, 1992.

[17] J. G. G. Ramos, D. Bazeia, M. Hussein, and C. Lewenkopf, "Conductance peaks in open quantum dots," *Physical review letters*, vol. 107, no. 17, p. 176807, 2011.